ACS APPLIED NANO MATERIALS

Subscriber access provided by UNIV OF NEW ENGLAND ARMIDALE

Article

Tailoring the dielectric and mechanical properties of polybutadiene nanocomposites by using designed ladder-like polysilsesquioxanes

Massimiliano D'Arienzo, Sandra Diré, Veronica Masneri, Davide Rovera, Barbara Di Credico, Emanuela Callone, Simone Mascotto, Alessandro Pegoretti, Fabio Ziarelli, and Roberto Scotti

ACS Appl. Nano Mater., **Just Accepted Manuscript** • DOI: 10.1021/acsanm.8b00558 • Publication Date (Web): 13 Jul 2018

Downloaded from http://pubs.acs.org on July 14, 2018

Just Accepted

"Just Accepted" manuscripts have been peer-reviewed and accepted for publication. They are posted online prior to technical editing, formatting for publication and author proofing. The American Chemical Society provides "Just Accepted" as a service to the research community to expedite the dissemination of scientific material as soon as possible after acceptance. "Just Accepted" manuscripts appear in full in PDF format accompanied by an HTML abstract. "Just Accepted" manuscripts have been fully peer reviewed, but should not be considered the official version of record. They are citable by the Digital Object Identifier (DOI®). "Just Accepted" is an optional service offered to authors. Therefore, the "Just Accepted" Web site may not include all articles that will be published in the journal. After a manuscript is technically edited and formatted, it will be removed from the "Just Accepted" Web site and published as an ASAP article. Note that technical editing may introduce minor changes to the manuscript text and/or graphics which could affect content, and all legal disclaimers and ethical guidelines that apply to the journal pertain. ACS cannot be held responsible for errors or consequences arising from the use of information contained in these "Just Accepted" manuscripts.

ACS Publications

is published by the American Chemical Society. 1155 Sixteenth Street N.W., Washington, DC 20036

Published by American Chemical Society. Copyright © American Chemical Society. However, no copyright claim is made to original U.S. Government works, or works produced by employees of any Commonwealth realm Crown government in the course of their duties.

Tailoring the dielectric and mechanical properties of polybutadiene nanocomposites by using designed ladder-like polysilsesquioxanes

Massimiliano D'Arienzo[1], Sandra Diré[2,3]*, Veronica Masneri[1], Davide Rovera[1], Barbara Di Credico[1], Emanuela Callone[2,3], Simone Mascotto[4], Alessandro Pegoretti[2], Fabio Ziarelli[5], Roberto Scotti[1]*

[1] Department of Materials Science, INSTM, University of Milano-Bicocca, Via R. Cozzi 55, 20125 Milano, Italy.

[2] Department of Industrial Engineering, University of Trento, via Sommarive 9, 38123 Trento Italy

[3] "Klaus Müller" Magnetic Resonance Laboratory, DII, University of Trento, via Sommarive 9, 38123 Trento Italy

[4] Institut für Anorganische und Angewandte Chemie, Universität Hamburg, Martin-Luther-King-Platz 6, 20146 Hamburg, Germany

[5] Aix-Marseille Université, CNRS, Fédération Sciences Chimiques, Spectropole Campus Scientifique de Saint Jérôme - 13397 Marseille Cedex 20, France

KEYWORDS

Nanocomposites, silsesquioxanes, dielectric properties, hybrid materials, interfaces, mechanical properties

ABSTRACT

In this study, the preparation of polybutadiene/polysilsesquioxane nanocomposites (NCs) having tunable thermomechanical and dielectric properties is reported. This was achieved by using different amounts of a filler consisting of a silsesquioxane with a defined ladder-like molecular structure (LPMASQ) bearing reactive methacrylate functionalities.

In detail, solid-state nuclear magnetic resonance NMR investigation revealed that an increasing amount of filler leads to a progressive homopolymerization of LPMASQ units resulting in the generation of domains in the composites, which induce a kind of polymer chain confinement in proximity of the hybrid interface. The evolution of the molecular organization of the inorganic nanobuilding blocks as a function of their concentration has been highlighted also by small-angle X-ray scattering (SAXS) experiments.

The gradual assembly of LPMASQ units gives rise to peculiar dielectric properties along with enhanced thermal and mechanical stability of the final NCs, thus being suitable to supply materials for applications in high performance dielectrics. Furthermore, these outcomes support the idea that a careful control of the molecular architecture and organization of the silsesquioxanes in a polymer matrix allows to simultaneously modulate two or more distinct functional features of polymer NCs.

INTRODUCTION

Over the past decades, the research on polymer NCs have stimulated enormous efforts in the development of novel and improved functional properties. In this class of materials, the characteristics of the singular components (*i.e.*, polymer, nanoparticles, molecular additives) can be easily tailored in order to incorporate the most advantageous properties into the final composite[1,4]. The features of the NCs generally rely on those of the individual building blocks (*e.g.*, structure, morphology, and surface functionalization of filler particles, type and nature of polymer matrix) and on their architecture or assembly [1, 2]. Furthermore, their often innovative features largely emerge from the synergism among the inorganic and organic components and by engineering of the filler/polymer interface [3,4].

In comparison to conventional nanoparticles the usage of silsesquioxanes (SSQs) as fillers in polymer NCs can be very beneficial. It has been demonstrated that the incorporation of SSQs can, for instance, considerably upgrade both thermomechanical stability and chemical resistivity of the polymers, and that even their degree of biocompatibility exceedingly increases [5-13].

SSQs are hybrid compounds with general formula $[RSiO_{1.5}]_n$ (R = H, alkyl, aryl or alkoxy). The structural core of the Si–O–Si network dictates the final structure of the SSQs. They can be classified into as either random or random-branched macromolecules, polyhedral oligomeric silsesquioxanes (POSS), and ladder-like polysilsesquioxanes (LPSQs)[9,14]. Only POSS and LPSQs display a tuneable architecture, which delivers unique functional properties [15,16].

In this frame, Matejka et al.[17] synthesized hybrid NCs by combining a diepoxy-functionalized POSS monomer with epoxy resins proving that both filler loading and POSS unit arrangement govern the final properties of the composite. In detail, they observed that the POSS units form

crystalline lamellae by self-assembling in the resin, behaving as junctions of the polymer chains, which restrict their mobility, thereby determining a significant mechanical reinforcement [17].

LPSQs are polymeric analogues of POSS where Si–O–Si bonds form a double-stranded ladder-like structure[14]. Their high molecular weight, condensation degree and structural regularity, provide improved mechanical, thermal, dielectric properties and deliver outstanding compatibility with polymeric matrix[18-23].

In this context, we have recently studied the properties of polybutadiene enclosing thiol-functionalized SSQs nano-building blocks (SH-NBBs) with tailorable functionality and structure (cage or ladder-like) [24]. Swelling and NMR experiments revealed the influence of both SH-NBBs loading and ladder-like architecture on the structure and mobility of the polymer chains, and on the mechanical features of NCs. These changes suggest the existence of bonding interactions at the organic-inorganic interface[24]. In another recent study, Cho et al.[25] prepared polyvinylidene fluoride (PVDF)/UV-curable LPSQ composites. The LPSQs enclosed phenyl and methacrylate groups, which enabled hydrogen-bonds with PVDF backbone enhancing not only the reinforcement, but engendering also a tuning of the dielectric properties of the composites[25].

Currently, SSQs (*e.g.*, POSS) have received extensive attention as fillers capable of tuning the permittivity (*i.e.*, dielectric constant, ε_r) of polymer NCs, which simultaneously leads to a strengthening of their thermal and mechanical robustness[5,25-27]. Yang et al.[28] developed a series of novel NCs by the hydrosilylation reaction of octahydridosilsesquioxanes with several α,ω-dienes of different chain length, which lead to organic/inorganic (O/I) networks in which the two kinds of monomers are chemically bonded to each other. The resultant polymeric layers displayed improved mechanical features and lower dielectric constant ($\varepsilon_r \sim 2.43$), which has been achieved by exploiting the nanoporosity imparted by the POSS units[28]. This suggests the

possibility of tuning dielectric and mechanical properties by tailoring either molecular structure or assembly of the SSQs.

The enhancement of polymer-SSQs NCs features, depending on the filler loading, the degree of dispersion, their molecular architecture (ladder, cage), structural organization and assembly, and the chemical nature of the pendant groups, has been extensively reported in the literature [5-27]. However, the control of the filler characteristics and the investigation of their influence on the hybrid interface are still challenging tasks, especially in view of designing polymer nanocomposites for applications in high performance dielectrics, where the combination of improved mechanical strength and tailorable permittivity are essential requirements[2].

Stimulated by this background, we carefully studied the incorporation of ladder-like molecular SSQs bearing specific and reactive functional groups in a polymer host. The main focus of the study lies on the effects of the filler amount and molecular assembly on the mobility of the polymeric chains and, in turn, on the dielectric and thermomechanical features of the resulting composite materials. Among the polymers, we selected *cis*-1,4-polybutadiene (PB), for which the tailoring of dielectric and thermomechanical properties represents a key point for many large-scale applications, like tires, wire cables and conveyor belts.

In detail, a totally condensed, ladder-like structured poly(methacryloxypropyl)silsesquioxane with a medium degree of structural regularity (LPMASQ) synthesized through an easy one-pot procedure[16,23] was employed as a suitable filler for producing PB NCs by a *solution-blending* technique[10]. The thermal properties of the synthesized NCs were determined by thermogravimetric analysis (TGA). The interactions between LPMASQ and polymer were investigated by solid-state NMR spectroscopy. Furthermore, the specific organization and the assembly of LPMASQ units in the polymer matrix have been inspected by SAXS. Finally,

dielectric and mechanical features of the novel NCs were examined by impedance spectroscopy and dynamic mechanical thermal analysis (DMTA) measurements. The results evidenced significant modifications of both the structural organization of the LPMASQ and the mobility of the polymer chains with increasing filler loading, which induce peculiar dielectric and mechanical features.

EXPERIMENTAL

Materials

3-methacryloxypropyltrimethoxysilane (TMMS), tetrahydrofuran (THF), azobisisobutyronitrile (AIBN), polybutadiene *cis* average M_w 200000-300000 (PB) and toluene were obtained from Sigma–Aldrich and used without further purification.

Synthesis of LPMASQ

The preparation of LPMASQ was carried out as reported in reference 23. In detail, potassium carbonate, K_2CO_3 (0.04 g, 0.29 mmol) was dissolved in 4.8 mL of H_2O and 9.0 ml of THF. Then, 3-methacryloxypropyltrimethoxysilane (0.08 mol) was added dropwise under nitrogen flow and the clear solution was left under stirring reacting at room temperature (RT) for 240 h. No precipitation was ever observed during the considered reaction time. An almost transparent and jelly-like LPMASQ (15.2 g, 95% crude yield) was obtained by solvent evaporation. The ladder-like structure of the LPMASQ was determined by Fourier-transform infrared spectroscopy (FT-IR) and NMR experiments.

Preparation of NCs

NCs were produced by including LPMASQ into PB with the procedure ~~shown~~ reported in Scheme 1. Pre-dried PB (2 g) was dissolved in 20 mL of anhydrous toluene at 333 K. Then, suitable amount of LPMASQ (3, 5, 7.5, 10, 15, 25, 40 wt. %) and AIBN (0.02 g) were mixed to the hot PB solution at 333 K for different reaction times (2-48 h) under N_2 flow. The solutions were cast in Petri dishes, and volatile solvent and by-products were eliminated by evaporation under aspiration hood and then by heating the samples at 70 °C for 1 hour under vacuum (p < 3 mbar).

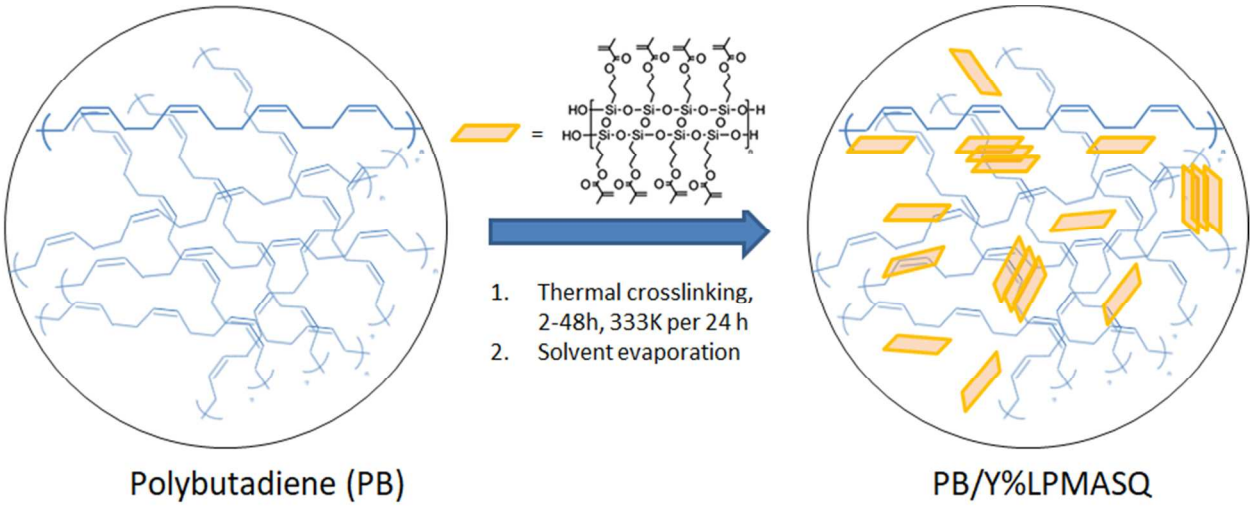

Scheme 1. Synthesis of PB/Y%LPMASQ NCs

NCs will be labeled PB/Y%LPMASQ_Xh where Y represents the percentage of LPMASQ (Y = 3, 5, 7.5, 10, 15, 25, 40 wt. %), and X the reaction times (Xh = 2-48 h). Moreover, 1 g of LPMASQ was dissolved in toluene. The homopolymerization reaction was run for 24 h by adding the suitable amount of AIBN (0.025 g), as described above for the NCs preparation. The homo-polymerized LPMASQ_24h sample was investigated by FTIR and NMR spectroscopy.

Characterization of PB/Y%LPMASQ_Xh NCs

(ATR)-FTIR measurements in attenuated total reflection (ATR) modus were carried out by a Perkin Elmer Spectrum 100 instrument. The profile fitting analysis was performed on the spectra recorded on pristine and polymerized LPMASQ and PB in the range 1900 – 1500 cm^{-1} using Dimfit software [29].

Scanning electron microscopy (SEM) measurements of the NCs were performed by a Vega TS5136 XM Tescan microscope under high vacuum. In order to get the best reliability from the investigation, at least 10 images for each nanocomposite in different sample region were acquired.

Magic angle spinning (MAS) NMR experiments were performed with a Bruker 300WB spectrometer (^{1}H frequency: 300.13 MHz, spinning rate 7 and 10 kHz). The NMR experiments were run on PB/Y%LPMASQ_24h nanocomposites, and on pristine and homo-polymerized precursors, produced using the same conditions applied for the nanocomposite preparation. Both proton decoupled single pulse (SP) and cross polarization (CP) pulse sequences were used. Experimental conditions: ^{13}C (75.47 MHz), SP pulse width 3.5 μs (π/2), decoupling length 5.9 μs, recycle delay 30 s, 1k; CP contact times 0.3, 0.5, 1, 2, 3, 6, 9 ms and recycle delay 5 s. ^{1}H pulse width 4 μs, recycle delay 5 s, 16 scans. Relaxation experiments were run on a Bruker Advance III 400MHz using saturation-recovery pulse sequence with variable relaxation delay in the range 0.001-20 s and spin-lock pulse sequence with variable spin-lock pulse in the range 0.5 – 500 ms (a frequency field of 70 kHz was used for the spin-lock field B1). Both experiments were run at 293 and 263 K in order to evaluate possible different behaviors. The lineshape analysis was performed using Bruker TopSpin software and the fitting was considered acceptable with confidence level of 95%.

Basic MAS and CPMAS experiments were recorded to identify and evaluate any possible variation of the signals assigned to both LPMASQ and PB. Moreover, ^{13}C Cross Polarization (CP) at different contact times and ^{1}H relaxation experiments were carried out in order to achieve further insights. In fact, interactions at the interface in composite materials affect strongly also other intrinsic parameters, such as conformation and mobility that depend both on homonuclear and heteronuclear interactions. Accordingly, the proton spectrum intensity (*M*) as a function of the repetition time (*t*, interval between two π/2 pulses) has been measured with the saturation recovery pulse sequence. Moreover, the proton spectrum intensity (*M*) as a function of the spin-lock pulse duration (*t'*, interval in which the magnetization is locked in the rotating frame and decays) can be determined through the spin-lock pulse sequence. The M decay curves are described by Equations 1 and 2, respectively, which allow to calculate the relaxation parameters, T_{1H} (spin-lattice relaxation time) and $T_{1\rho(H)}$ (spin–lattice relaxation time in the rotating frame).

$$M(t) = M_0(1 - e^{-\frac{t}{T_{1H}}}) \quad (1)$$

$$M(t') = M_0 \cdot e^{-\frac{t'}{T_{1\rho H}}} \quad (2)$$

T_{1H} and $T_{1\rho(H)}$ are related to different frequency ranges and therefore their values are sensitive to molecular motions on different time scales. T_{1H} and $T_{1\rho(H)}$ values are calculated by fitting the experimental curve with single or multiple exponential laws depending on homogeneity, segregation and/or domain size [30].

SAXS measurements were performed by an IncoatecTM X-ray source ImS with Quazar Montel optics, under experimental conditions already reported in previous study [31].

TGA measurements were accomplished with a Mettler Toledo TGA/DSC1 STARe system under the same experimental conditions reported in reference 24.

DMTA measurements were run on a DMA Q800 (TA Instruments, New Castle, DE, USA), under the same experimental conditions reported in our previous study [24].

RESULTS

Characterization of LPMASQ and PB/Y%LPMASQ_Xh Nanocomposites

The synthesised LPMASQ have the same structural characteristics as reported in ref. 22-23 and 32-33, as evidenced by the results of the FT-IR and ^{1}H NMR investigations reported in Fig. S1 and S2 (Supporting Information). In particular, the acrylate-substituted LPMASQ studied in the present work, have flexible substituents and belong to "medium-degree regular" LPMASQ, if compared to highly regular template-route phenyl-LPMASQ[34] or to phenyl-silsesquioxane resins with different degrees of ordering[35]. A dominant ladder-like structure can be expected for the studied acrylate-LPMASQ, while some structural irregularity in combination with flexible substituents should favor higher solubility and easier blending with polybutadiene.

The LPMASQ incorporation in PB was initially examined by FT-IR (Fig. 1). The spectra of PB before and after the insertion of 15 and 25 wt. % LPMASQ (i.e. PB/15%LPMASQ_24h and PB/25%LPMASQ_24h) are reported in Figure 1a.

With increasing filler amounts, the vibrations associated to LPMASQ units become slightly more evident, in particular in the range between 1200- 900 cm^{-1}. Further, a detailed analysis of the FT-IR spectra of the NCs reveals two different vibrations of the C=C bonds of LPMASQ and PB at 1638 and 1656 cm^{-1}, respectively (Fig. 1b). The same results have been obtained for PB/Y%LPMASQ_24h NCs (not reported). The change in relative intensity of the signals due to Si-O asymmetric stretching vibrations suggests a partial rearrangement of the incorporated silsesquioxane units inside the polymer matrix in comparison to pure LPMASQ. This hypothesis

is supported by the FT-IR spectrum of the homo-polymerized LPMASQ_24h sample (Fig. S3), showing both the shift of the signals to 1126 and 1040 cm^{-1} and an increase of the peak intensity at 1126 cm^{-1}. These spectral modifications are reflecting changes in Si-O-Si angles that are generally associated with the formation of cage-like silsesquioxane structures. The LPMASQ assembly resulting from crosslinking of acrylate groups belonging to either the same molecule or to neighboring LPMASQ molecules could lead to the formation of "cages substructures" with a similar effect on Si-O stretching vibrations.

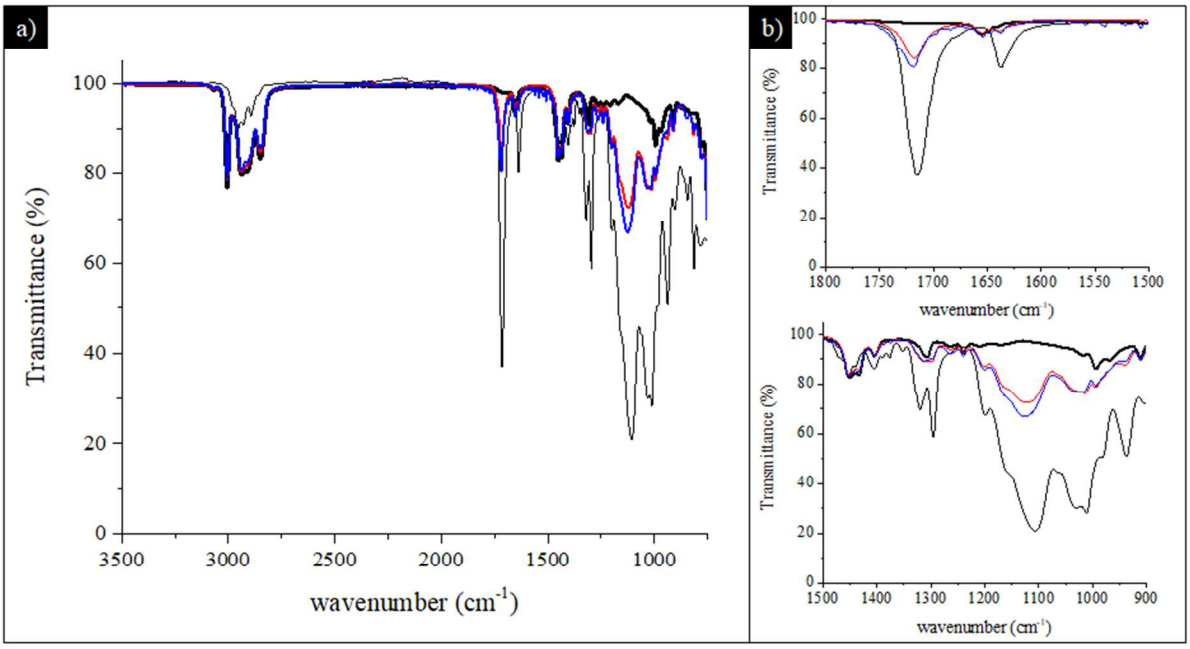

Figure 1. a) FT-IR spectra of pure PB (bold black line), as-prepared LPMASQ (black line), PB/15%LPMASQ_24h (red line) and PB/25%LPMASQ_24h (blue line) NCs; b) magnifications of the methacrylate (top) and of the siloxanes (bottom) spectral regions.

The comparison of C=O and C=C signals in as-prepared and polymerized LPMASQ strengthens this hypothesis. The high polymerization capability of LPMASQ is proven by the strong decrease of the C=C bond vibration. The profile fitting analysis performed in the range 1900-

1530 cm^{-1} (Fig. S4) gives a residual of 7% unreacted C=C bonds. Moreover, the shape of the carbonyl signal, which in as-prepared LPMASQ can be sufficiently well simulated with a single component, becomes much more complex in the polymerized sample. The best fit of signal was obtained by at least three carbonyl signal components are required, which are consistent with C=O groups in different chemical environments.

The possible effect of the reaction time on the NCs properties was assessed by a comparison among the FT-IR spectra of PB NCs loaded with 15 wt. % of LPMASQ, obtained after 2, 12, 24 and 48 h of reaction, has been performed (Fig. 2).

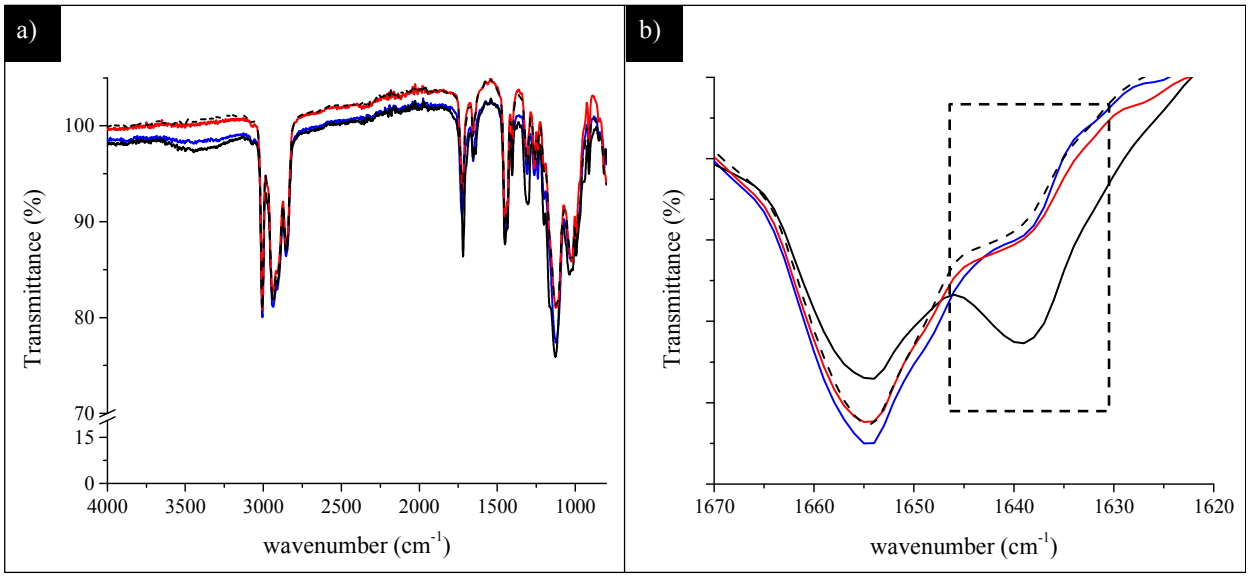

Figure 2: a) FT-IR spectra of PB/15%LPMASQ_2h (black line), PB/15%LPMASQ_12h (blue line), PB/15%LPMASQ_24h (red line) and PB/15%LPMASQ_48h (black dashed line); b) magnification of the C=C stretching mode. Dashed region in inset highlights the change of the C=C bond vibration of LPMASQ.

The LPMASQ structure appears substantially unaffected by the reaction time. Accordingly, the ν_{as}(Si-O) signal in the range 1200-900 cm^{-1} related to the ladder-like species do not show

appreciable changes (Fig. 2a). More interestingly, a decreasing intensity of the signal of the C=C vibrations with increasing reaction times can be detected, in particular, for the signal originating from the methacrylate groups of LPMASQ (Fig. 2b). These effects become relevant for samples reacted at least 24 h and may be associated with the condensation among LPMASQ units, which will be pointed out below in the discussion of the NMR results.

In conclusion, the FT-IR results, assess the effective LPMASQ incorporation in the PB matrix, suggesting a dissimilar structural arrangement of LPMASQ in the NCs as a function of the filler loading.

The morphological features of the NC materials were investigated by SEM microscopy. In detail, micrographs were collected for PB/Y%LPMASQ samples prepared with different reaction times. Figure 3 (top) shows typical images obtained for PB/15%LPMASQ NCs. The presence of numerous white shaded spots of micrometer or sub-micrometer size almost uniformly dispersed in the matrix can be observed at short reaction times (t = 2h). As the time increases up to 12 h, they progressively disappeared and at t = 24-48h they are substantially absent. A similar behavior has been detected for NCs loaded with 10, 25 and 40 wt. % of LPMASQ, while for lower loadings (*i.e.*, 3, 5 and 7.5 wt. %) no significant outcome could be derived from the SEM investigation.

These results have been interpreted by suggesting the initial formation of a kind of microemulsion upon incorporation of LPMASQ units into the PB matrix, most likely associated with the amphiphilic nature of the filler, which is composed of a more hydrophilic silica-based core and a rather hydrophobic surrounding of methacrylate functionalities with a high affinity towards the PB matrix. This hypothesis is supported by EDAX analysis (Fig. 3 bottom), which

reveals that Si is the most abundant element inside the white-shaded spots, while C is the main element in the surrounding matrix. Moreover, the observed spherical or spheroidal shapes suggest that these micro objects are or have been plastically deformable at least at the time of their formation.

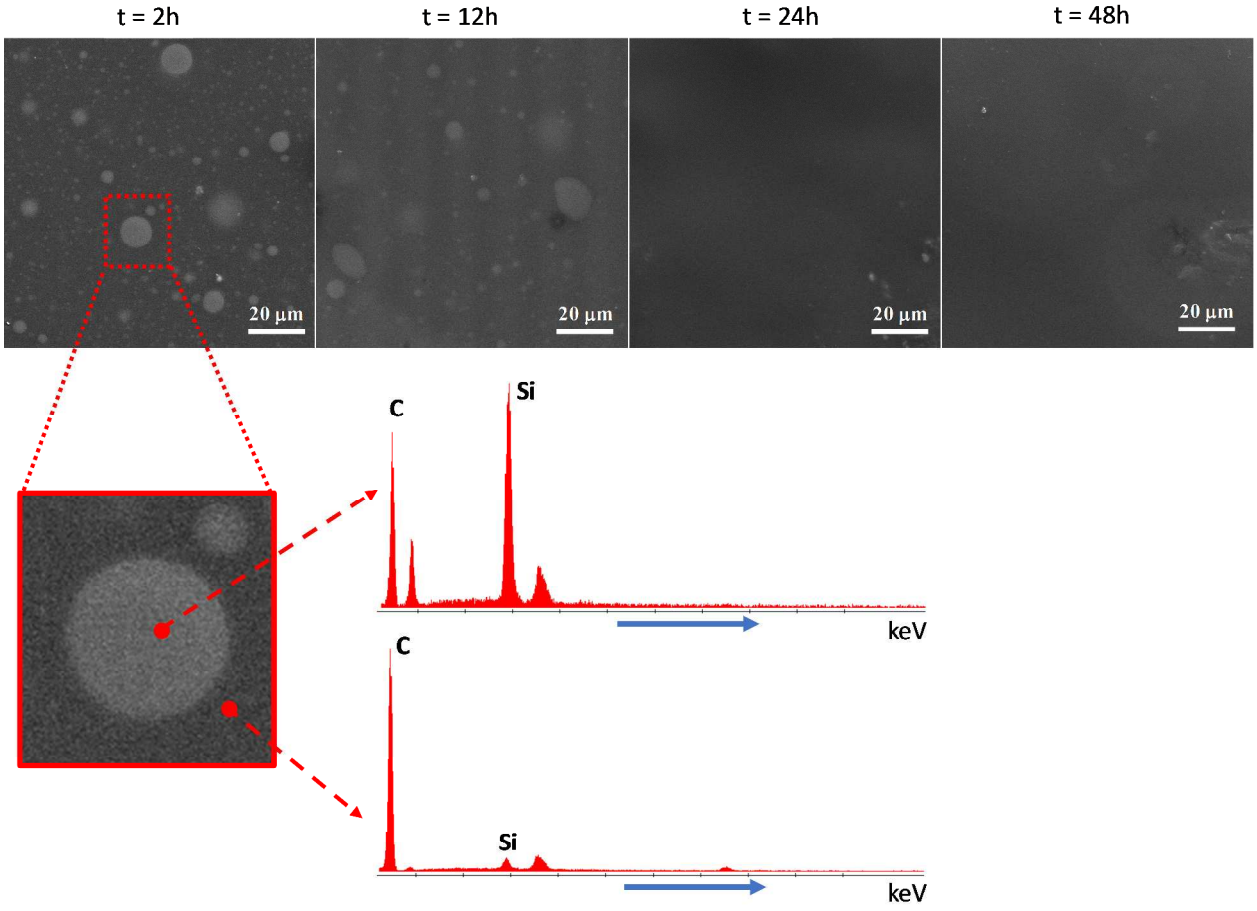

Figure 3: top) SEM micrographs of PB/15%LPMASQ nanocomposites obtained at different reaction times; bottom) magnification of the white shaded spots observed for reaction time < 24 h emulsions in PB/Y%LPMASQ NCs and typical EDAX spectra acquired in the corresponding regions.

As the reaction at 333 K in the presence of AIBN (see Experimental section) proceeds, methacrylate functionalities can be easily activated. This may promote homogenization via reaction blending, including connection of LPMASQ units among each other to larger oligomeric structural units as a result of reactions of the acrylate groups, as well as reactions of the pending acrylate functions of LPMASQ with suitable C=C double bonds of the PB matrix. Accordingly, SEM/EDAX Si elemental maps of the NCs recorded at different reaction times (see Figure S5, Supporting Information), revealed a rather homogeneous distribution of Si in the matrix after 24 h.

Although clear evidences on the filler dispersion and organization in the PB at the submicrometer scale were not achieved at this stage, these results suggest that the best reaction time enabling a suitable compatibilization and distribution of LPMASQ in the polymer matrix should be approx. 24 h. Therefore, all further characterizations were performed exclusively on PB/Y%LPMASQ_24h NCs.

A deeper understanding how the LPMASQ units are incorporated into the PB matrix was achieved byvarious ^{13}C solid state NMR experiments on PB/Y%LPMASQ_24h nanocomposites, pristine and homo-polymerized PB and LPMASQ.

The ^{13}C CP MAS spectra of pure and homo-polymerized LPMASQ are shown in Figure 4a and b, respectively. The scheme in the inset of Figure 4 reports the C labeling used for peak assignment, based on the literature[23, 36, 37]. In the pristine LPMASQ (Fig. 4a) the resonances due to the methylene carbon atoms in the propyl chain (**a, b, c**) and the methacrylate tail, *i.e.* carbonyl (**d,** 165 ppm), vinyl (**e** and **g** at 135 and 124 ppm respectively) and methyl (**f**) C atoms, can be clearly recognized. The polymerization activated by AIBN (Fig. 4b) is proven by the

strong reduction in intensity of the signals attributed to the methacrylate double bond (**e** and **g**), and the appearance of both a peak at 45 ppm (**e'**, **g'**) and a second carbonyl resonance, which is downfield shifted (**d'**, 175 ppm) with respect to the one present in the pristine LPMASQ (**d**, 165 ppm). The fact that at least two different carbonyl species are present in the sample agrees with the conclusions drawn from the FT-IR study on the polymerized LPMASQ sample.

The spectrum of the sample PB/10%LPMASQ_24h, which is representative for all spectra of the NCs, independent of the amount of loading with LPMASQ, is shown in Figure 4c.

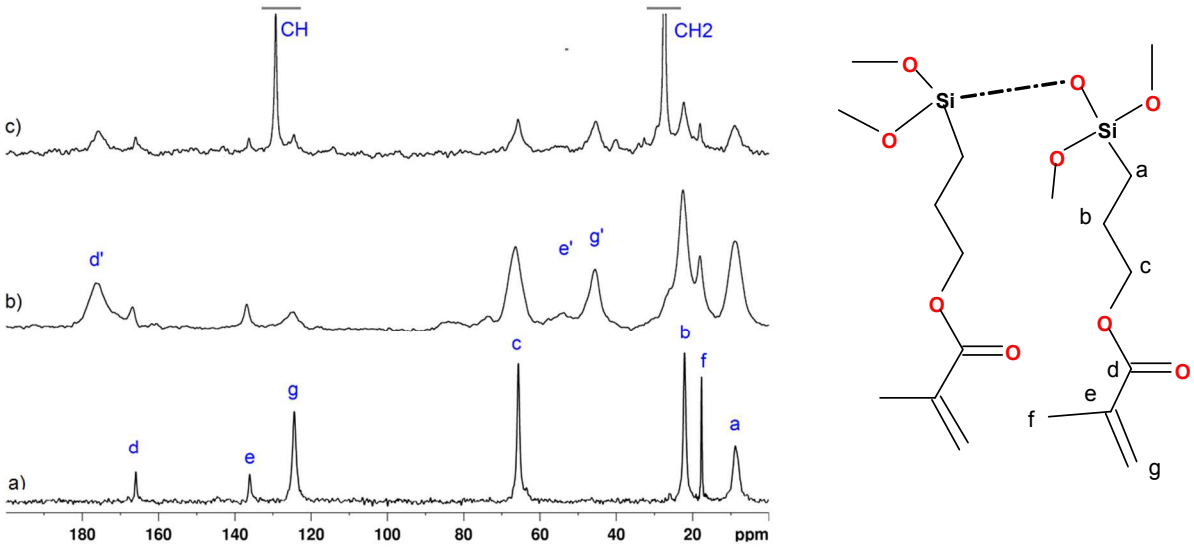

Figure 4: ^{13}C CP MAS NMR spectra of a) pristine LPMASQ, b) homo-polymerized LPMASQ and c) PB/10%LPMASQ_24h.

The pristine commercial polymer PB displays two main narrow signals (129.5 and 27.6 ppm), respectively, due to =CH and -CH_2- functional groups in *cis*-1,4-configuration (Figure S6). The sharpness of these resonances is due to the high mobility of the functional groups, leading to the averaging of nearly all dipolar and chemical shift interactions[24]. Furthermore, the weak peaks

due to carbons in or adjacent to 1,2-unit (v) and trans-1,4-units (t) are observable. The methyne carbon resonance in 1,2-units (v) occurs at 41 ppm, while the olefinic carbons of 1,2-units give rise to signals at -114 (=CH_2) and -142 (-CH=) ppm[24]. The spectrum of the nanocomposite (Figure 4c) shows the typical resonances of both PB and LPMASQ.

Moreover, as observed for homo-polymerized LPMASQ (Figure 4b), the appearance of the peaks attributed to **e'**, **g'**, and **d'** and the reduced intensity of **e** and **g** peaks prove that the polymerization reaction effectively occurred. The presence of both **d** and **d'** resonances can be used to quantify the extent of the polymerization reaction, since the CP MAS experimental conditions have been selected in order to give the maximum intensity of both signals. The degree of polymerization can be calculated by the integral intensities of the signals **d** and **d'** and is given by the ratio d'/(d+d'). The obtained values summarized in Table1 show that the degree of polymerization increases with increasing amount of LPMASQ filler in the nanocomposite (the ^{13}C CPMAS spectra of the PB/Y%LPMASQ_24h samples are shown in Figure S7A).

Table 1. Degree of polymerization of PB/Y%LPMASQ_24h samples calculated from the integrated area of carbonyl resonances in the NMR spectra shown in Figure S7.

LPMASQ amount (wt. %)	d' area % = d'/(d+d') ± 2 %
25	92.0
15	77.0
10	67.0
5	ND
3	ND

The value calculated for homo-polymerized LPMASQ is about 95% (in good agreement with the result obtained by FT-IR), thus indicating the large ability to polymerize the propyl-methacrylate groups in the silsesquioxane filler. Unfortunately, due to the low S/N ratio the degree of cross-

linking cannot be calculated for samples PB/3%LPMASQ_24h and PB/5%LPMASQ_24h (see Table 1).

The line shape of the PB peaks in PB/10%LPMASQ_Xh NCs (Fig. 4c) does not show any appreciable difference with respect to the one of pristine PB, and therefore no direct indication on the possible co-polymerization between PB and LPMASQ can be derived from the spectra.

However, occasional co-polymerization reactions between the vinyl groups of PB and the acrylate functions of LPMASQ cannot be excluded, in particular taking into account the well-known high reactivity of 1,2-vinyl units, which are present in the pristine PB in a 2% amount[24]. Furthermore, this hypothesis could also explain the homogenization observed through SEM analysis with increasing reaction blending time over 24 hours.

To get some more insight on the possible filler-matrix interactions, experiments on proton relaxation and magnetization transfer were carried out, aiming to highlight any possible spatial heterogeneity of the NCs.

As detailed in the experimental section, the measurement of the spin-lattice relaxation time (T_{1H}) and spin-lattice relaxation time in the rotating frame ($T_{1\rho(H)}$) of the abundant proton spins allows to get information on molecular motions on different time scales. Fast molecular motions taking place at short range are described by $T_{1(H)}$ values, whereas $T_{1\rho(H)}$ is related to slower motions typical of the dynamics of long chains[30]. Both motions are usually averaged by spin diffusion over short distances giving hints about component mixing [38]. In homogeneous materials very similar $T_{1\rho(H)}$ values are determined. Oppositely, different $T_{1\rho(H)}$ values can be detected when domains with sizes larger than the spatial averaging by spin-diffusion occur.

Thus, both T_{1H} and $T_{1\rho}(H)$ were measured for the signals of CH and CH_2 protons belonging to polybutadiene chains (PB/Y%LPMASQ_24h ^1H spectra shown in Figure S7B). Figure S8A and

B show the trend of magnetization intensity vs. spin-lock time of the selected samples. The curves fitting gives the relaxation times reported in Table 2 for the experiments carried out at room temperature (similar results are obtained at 263K). T_{1H} values around 0.8s are found for all the samples, being indicative of a spin diffusion averaging. $T_{1\rho}(H)$ data, presented in Table 2, evidence that increasing filler loadings shortens the relaxation time, suggesting a dispersion of the LPMASQ on the nanoscale. Moreover, at filler loadings higher than 10%, the relaxation trend can be better described by two $T_{1\rho}(H)$ values, which account for heterogeneous systems with at least two domains. This evidence can be clearly recognized in Figure S8C, in which the logarithmic plot of magnetization vs. spin-lock time for PB/5%LPMASQ_24h and PB/25%LPMASQ_24h samples is shown. The two $T_{1\rho}(H)$ values indicate regions in which the polymer maintains its own mobility ($T_{1\rho}(H)$ close to the one of pure PB) and other regions characterized by very low $T_{1\rho}(H)$, highlighting the reduced mobility of polymer chains close to the interface with the LPMASQ cores.

The calculated ratio between mobile and rigid chains decreases with increasing the LPMASQ loading from 80/20 for PB/15%LPMASQ_24h to 70/30 for PB/25%LPMASQ_24h samples, respectively. This further confirms the interaction between PB and LPMASQ, indicating that more PB units are located at the interface between polymer matrix and LPMASQ segregated domains with increasing filler loadings.

Table 2. $T_{1\rho}(H)$ relaxation rates at 298K.

δ (ppm)	(-CH) 5.4	(-CH_2) 2.1
	$T_{1\rho}(H)$ (ms)	
PB pure	125	112
PB/5%LPMASQ_24h	118	105
PB/15%LPMASQ_24h	123/34	103/35
PB/25%LPMASQ_24h	62/10	54/8

Finally, the ^{13}C variable contact time (VCT) experiments have been recorded. In these experiments the signals of systems with high mobility increase in intensity with increasing the contact time, while signals related to systems with reduced mobility decrease. Figure 5 shows the ^{13}C CPMAS experiments recorded at various contact time for the representative PB/10%LPMASQ sample.

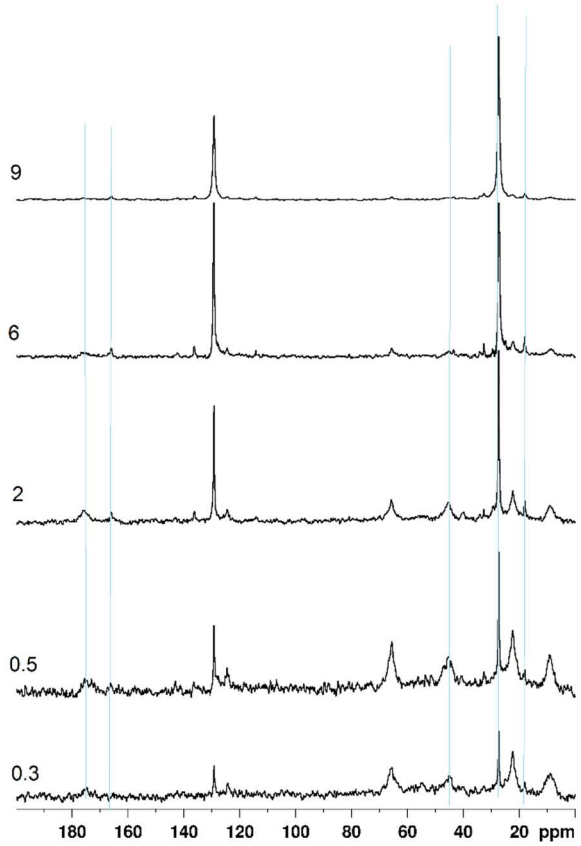

Figure 5: ^{13}C CPMAS NMR spectra of PB/10%LPMASQ_24h recorded at different contact times (0.3-9 ms, reported on every spectrum).

As can be seen, the signals due to the carbon atoms (**d', e', g'**), in polymerized LPMASQ and those due to the propyl carbons **a, b, c**, decrease in intensity at long contact times, indicating reduced mobility in the composites. The peaks **d** and **f**, belonging to the unreacted methacrylate

functions of LPMASQ, are visible at longer contact times, similarly to the signals of the PB chains, indicating high mobility. These results support the formation of LPMASQ domains in the composites, whose extent is not only related to filler loading but also to the high polymerization ability of LPMASQ.

In conclusion, the NMR results suggest that mainly weak interactions are established among PB chains and homo-polymerized LPMASQ, which assemble in domains whose size depend on filler loading.

The specific organization and the possible assembly of LPMASQ units in the polymer matrix has also been investigated by SAXS. The patterns obtained for PB/Y%LPMASQ_24h nanocomposites are summarized in Figure 6.

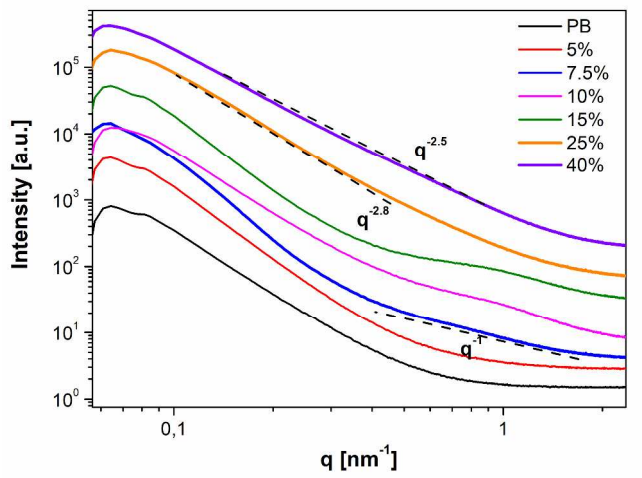

Figure 6: Scattering curves of the pure PB and of PB/Y%LPMASQ NCs with different filler amounts.

As a consequence of both the high structural complexity of the hybrid polymer formed by disordered organic and inorganic interpenetrating networks and the very low scattering contrast

between the silica and carbon-based phases, the patterns are very complex. The structural evolution of the composites with increasing LPMASQ amount can be studied by the variation of the curve shape. The homogeneous intensity decay observed at very low filler loadings, and the similarity to the curve of the pure polymer indicates a scarce contribution of the highly diluted LPMASQ units. Significant changes of the patterns are noticed between 7.5 and 15% loadings.

At $q > 0.4$ nm^{-1} the curves initially change their slope to q^{-1} showing the presence of rod-like objects[16], which can be attributed to the ladder-like structure of the silsesquioxanes. Successively, a weak shoulder at approximately $q = 1$ nm^{-1} appears, suggesting the existence of a short-range order among the inorganic nanobuilding blocks with a correlation length $d \approx 6$ nm ($d = 2\pi/q$). For higher LPMASQ loadings the scattering patterns show a constant non-integer slope of -2.8 and -2.5 for the 25 and 40 wt. % samples, respectively, which is typical of mass fractals [39, 40]. Hence, such amounts of filler loading promote closer interaction between the inorganic units, which aggregate together forming clusters of several tens of nanometers, probably constituting a continuous loose interpenetrated 3D network made of acrylate-connected LPMASQ and PB chains.

The dielectric properties of PB/Y%LPMASQ_24h NCs were evaluated by measuring the capacitance C according to the equation:

$$\varepsilon_r = C\, d/\varepsilon_0\, A \qquad (3)$$

(d = film thickness, A = area of the gold spot, $\varepsilon_0 = 8.854\ 10^{-12}$ F/m, vacuum permittivity).

Because the geometry of the setup of the electric measurements is of great importance, care was taken to perform the measurements on composites with almost the same thickness (680 ± 50 μm).

Moreover, the dielectric loss (tan δ), i.e. the ratio between imaginary component and the real component of the permittivity, has been calculated. The dielectric loss represents the material energy dissipation, thus, a material suitable for high performance dielectrics should have low tan δ values.

The main results are shown in Fig. 7. In detail, Fig. 7a shows the ε_r curves of the PB/Y%LPMASQ_24h n NCs as a function of frequency.

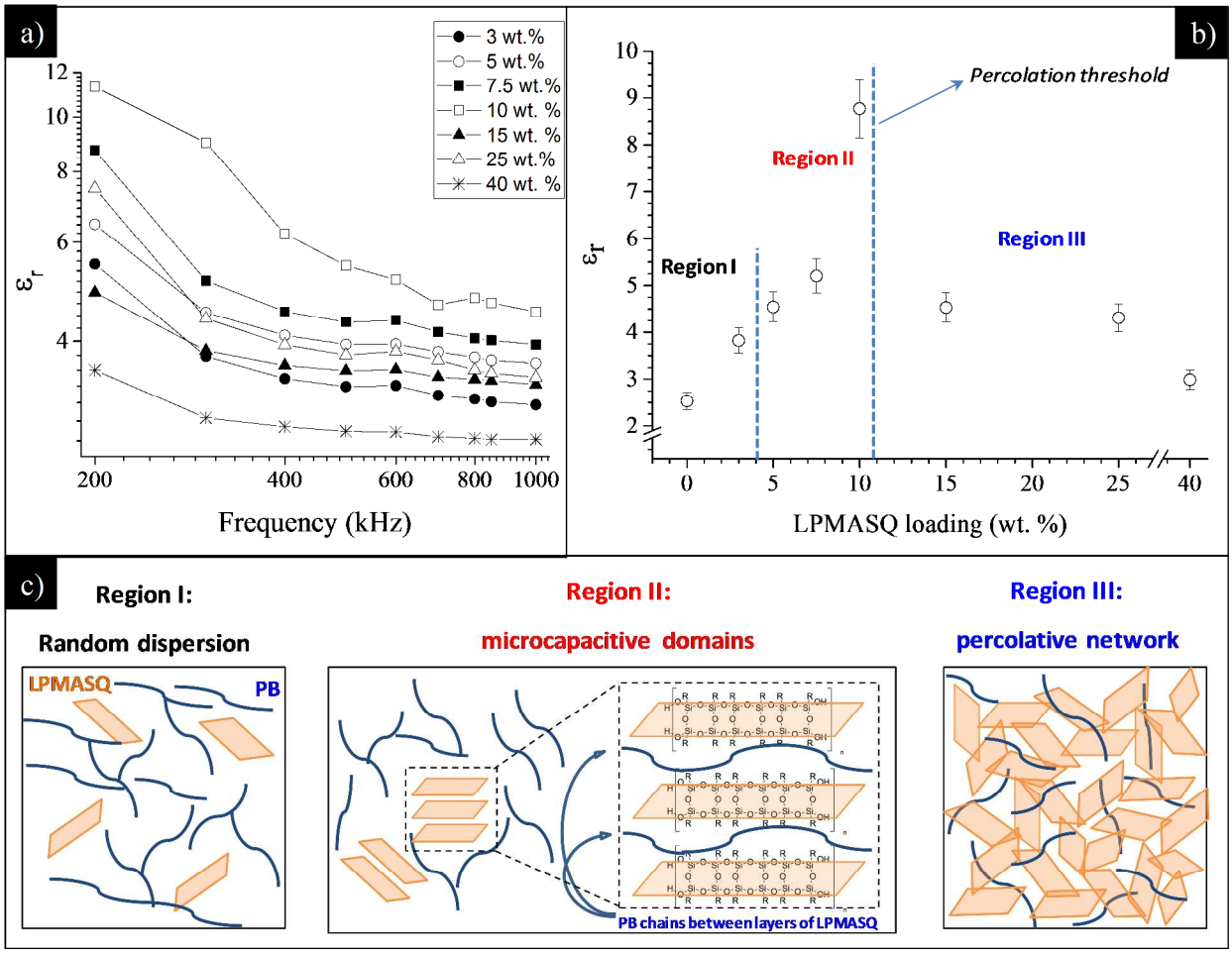

Figure 7: a) Trend of dielectric constant *vs.* frequency for PB/Y%LPMASQ_24h NCs; b) Trend of the dielectric constant of PB/Y%LPMASQ_24h composites *vs*. LPMASQ loading at 40 kHz (inset: LPMASQ loading in the composites); c) scheme of the NCs microstructures by increasing the LPMASQ concentration.

After an initial decrease between 20 and 40 kHz, it can be observed that the ε_r values for all samples do not show remarkable changes in the range of 40 - 100 kHz. This seems to indicate the absence of a high orientational polarization, as a consequence of the rigid structure of LPMASQ units which hinders the polymer mobility and the dipole alignment under an electric field. The calculated values of tan δ for all the NCs are lower than 0.2 (see Table S1, Supplementary Information). This result can be related to the dense polymer film, which totally embeds the LPMASQ units. This may generate an insulating layer able to reduce the charge mobility, increasing its resistance. Consequently, a low resistive current, which guarantees low dielectric loss and low energy dissipation, is expected below the percolation threshold.

The trend of the dielectric constant *vs.* the LPMASQ loading is depicted in Figure 7b. ε_r first increases when the LPMASQ fraction ranges from 0 to 5%, then sharply raises when the filler concentration is further increased reaching a maximum for a loading of 10 wt %. Finally, for LPMASQ percentages between 15 and 40 wt. %, ε_r value undergoes a significant drop.

These outcomes can be explained by the percolation theory and more specifically by ~~to~~ the Maxwell-Wagner model [41-45]. This theorizes the occurrence of microcapacitive structures with an increasing filler fraction within a matrix [41]. The microcapacitors, formed by adjacent filler particles and thin polymers interlayers [42], are partially connected in a parallel fashion and partially in a serial manner. The parallel-connected microstructures provide an increase of the material capacitance. Consequently, this leads to an increase of the local electric field intensity, favoring the accumulation of charge carriers at the filler–polymer interface [42]. This so-called Maxwell–Wagner effect [44], accounts for the remarkable enhancement of ε_r. At high filler amount, agglomeration phenomena occur, resulting in the generation of a continuous filler network (*i.e.*, percolation). This leads to the disruption of the capacitive microstructures and to

an inhomogeneous distribution of charges, with a consequent drop of the dielectric properties. Accordingly, the evolution of the dielectric properties as a function of filler loading shows three regions [45-47]. The first regards a very low filler amount, where the particles are randomly dispersed, and the dielectric constant only slightly rises with increasing filler loadings. The increase of filler amount induces the generation of microaggregates which act as microcapacitive structures, and thus, leading to a remarkable increase of ε_r. (*i.e.*, second region).

Finally, at high filler concentrations, the filler units are getting connected to each other generating a percolative network and consequently, the ε_r values decrease again (*i.e.*, third region) [48]. The percolation threshold lays almost between the second and the third region, and corresponds to the filler volume fraction at which the filler particles are connected throughout the whole matrix [49].

According to these observations and considering both SAXS and NMR results, we have tried to apply the Maxwell-Wagner model for explaining the dielectric behavior of PB/Y%LPMASQ_24h NCs as a function of the filler loading (Fig. 7b and 7c). In detail, at low LPMASQ concentrations, the slight increase of the dielectric constant has been related to the disordered distribution of PSQs in PB (region I in Fig. 7b and 7c).

Upon increasing the LPMASQ fraction up to 10 wt. %, a progressive LPMASQ homopolymerization and the occurrence of weak interactions among PB and the filler domains, possibly connected to a kind of polymer chains confinement take place. Along with these evidences, we may suggest that the assembly of ladder-like units promotes the formation of microcapacitors, constituted by neighboring LPMASQ units and thin layers of polymers in between (region II, Fig. 7c). The enhanced interfacial polarization provided by these structures, can be considered responsible of the remarkable increase of the ε_r values (see Fig.7b).

Beyond the percolation threshold (filler concentration > 10 wt. %), LPMASQ units tend to aggregate, forming object with higher dimensionality. It can be suggested that these aggregates become progressively interconnected generating a continuous interpenetrating network (region III in Fig.7c). This disordered filler organization probably leads to an inhomogeneous distribution of charge, which results in a rapid drop of the dielectric properties of the NCs (see Fig. 7b).

The influence of LPMASQ addition on the thermal properties of PB/Y%LPMASQ_24h NCs has been studied by TGA and DMTA. Figure 8 shows the thermal profiles of pure PB and of PB/Y%LPMASQ_24h NCs.

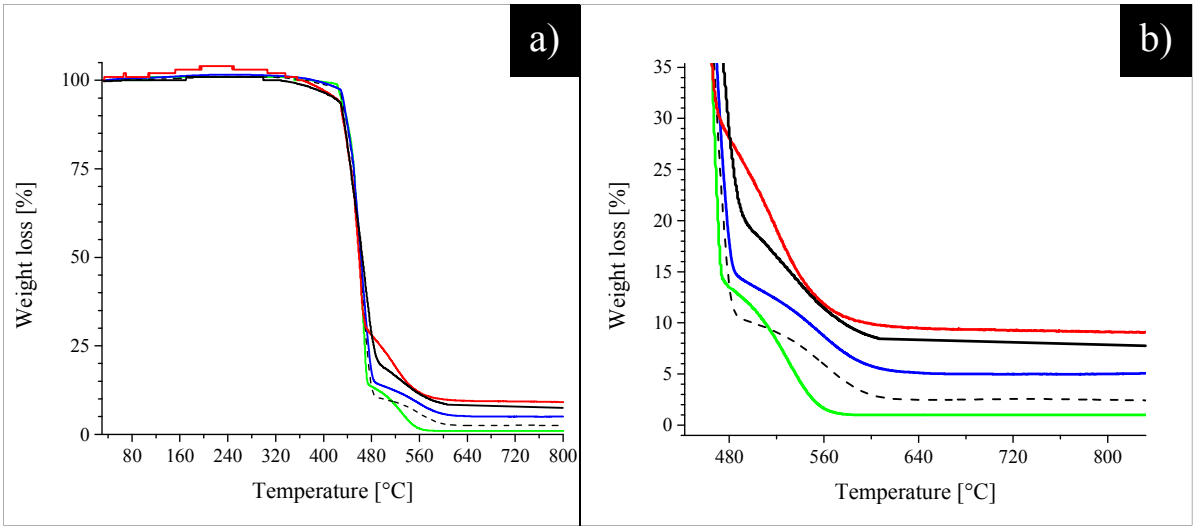

Figure 8: TGA curves of a) pure PB (green line), PB/3%LPMASQ_24h (black dashed line) and PB/10%LPMASQ_24h (blue line) and PB/15%LPMASQ_24h (black line) and PB/25%LPMASQ_24h (red line) b) highlight of the influence of LPMASQ loading on the thermal behavior on the NCs.

All samples display a remarkable weight loss from approx. 350 °C up to 480 °C. From 450 °C to 800 °C, a second weight loss occurs (Fig. 8a), which becomes less evident as the LPMASQ% in the composites increases, and clearly decreases for PB/25%LPMASQ_24h (see details in Figure 8b). This, beyond indicating the presence of remaining inorganic compounds (probably silica) at the end of the thermal evolution, points out an improved thermal stability of the PB matrix dependent on the LPMASQ concentration.

DMTA analysis of PB/Y%LPMASQ_24h NCs was run in order to explore the possible influence of the filler concentration on their mechanical properties.

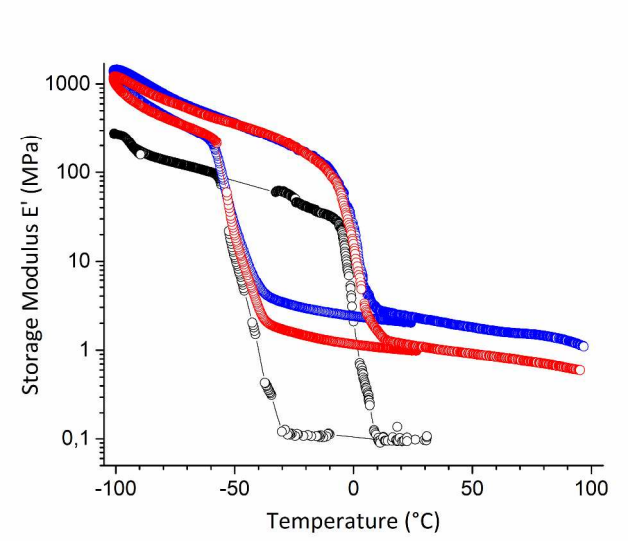

Figure 9. Trend of the storage modulus of pure PB (black line), PB/10%LPMASQ_24h (red line), and PB/25%LPMASQ_24h (blue line) NCs.

In particular, Fig. 9 reports the trends of the storage modulus E' vs. temperature of pure PB and of PB/10%LPMASQ_24h and PB/25%LPMASQ_24h NCs, which have been selected since their LPMASQ loadings lies just below and above the percolation threshold, respectively. It can be

clearly observed that, both above and below the glass transition temperatures, the introduction of LPMASQ in polybutadiene provides a remarkable stiffening of the polymer matrix. In fact, the storage modulus increases proportionally to the filler content (Fig. S9). A similar behavior has been obtained for PB/5%LPMASQ_24h and PB/15%LPMASQ_24h samples (not shown).

These results suggest that the progressive assembly of LPMASQ units in PB, as assessed by NMR and SAXS, actually supplies effective interactions (*i.e.*, filler-matrix entanglements) at the polymer-LPMASQ interface, which enable not only the tailoring of the dielectric properties, but also enhance the mechanical performances of the nanocomposites.

CONCLUSIONS

In this study, we investigated the incorporation of an unconventional filler LPMASQ, bearing reactive methacrylate groups and having a defined ladder-like molecular structure, into a in polybutadiene matrix. We focused on the effects of the loading and molecular organization on the mobilty of the polymeric chains, and, in turn, on the dielectric and thermomechanical features of the obtained NCs. The results of FT-IR and TGA investigations confirmed the successful incorporation of the filler into the polymeric host and highlighted an increase of the thermal stability with increasing filler amounts.

Solid-state NMR investigation revealed a progressive homopolymerization of LPMASQ units and the formation of filler domains in the composites, whose extent is not only related to the loading, but also to the high polymerization ability of LPMASQ. Interestingly, spin-lattice relaxation time measurements indicated a reduced mobility of PB chains in proximity of the hybrid interface, thus suggesting the occurrence of weak interactions among PB and the filler domains, possibly connected to a kind of polymer chains confinement induced by the LPMASQ

assembly. The evolution of the molecular organization of LPMASQ units in the polymer matrix as a function of their concentration has been also corroborated by SAXS measurements.

This progressive assembly of LPMASQ resulted in peculiar dielectric properties and in an enhanced mechanical reinforcement, suggesting the idea that controlling of the molecular structure of silsesquioxanes and its organization in the polymer matrix may potentially provide the possibility to develop suitable materials for applications in high performance dielectrics.

SUPPORTING INFORMATION

Details on the spectroscopic (FT-IR, and NMR) characterizations of LPMASQ and PB/Y%LPMASQ NCs are reported. This material is available free of charge via the Internet at http://pubs.acs.org.

AUTHORS INFORMATION

Corresponding Authors

* massimiliano.darienzo1@unimib.it, sandra.dire@unitn.it.

ACKNOWLEDGMENTS

A.P. thanks Miss Claudia Gavazza for her technical support in DSC and DMTA measurements. M.D. gratefully acknowledge Dr. Matteo Redaelli for his support in the NCs characterization and Prof. Alberto Paleari (UniMib) for useful discussion on dielectric properties. The LLP Erasmus+ mobility project of the European Commission promoted by the University of Trento is acknowledged for granting the stage in Marseille of Dr. E. Callone. S.M. thanks Dr. Andreas Meyer of the Physical Chemistry Institute of the University of Hamburg for performing the

SAXS measurements. Dr. Frank Hoffmann of the University of Hamburg is gratefully acknowledged for the critical reading of the manuscript.

REFERENCES

(1) Kao, J.; Thorkelsson, K.; Bai, P.; Rancatore, B. J. and Xu, T. Toward Functional Nanocomposites: Taking the Best of Nanoparticles, Polymers, and Small Molecules. *Chem. Soc. Rev*. **2013**, *42*, 2654–2678

(2) Kumar, S. K; Benicewicz, B. C.; Vaia; R. A.; Winey, K. I. 50th Anniversary Perspective: Are Polymer Nanocomposites Practical for Applications? *Macromolecules* **2017**, *50*, 714–731

(3) *Hybrid Materials: Synthesis, Characterization, and Applications*; Kickelbick, G., Eds.; Wiley-VCH: Weinheim, DE, 2007.

(4) *Functional Hybrid Materials*; Gómez-Romero, P.; Sanchez, C., Eds.; Wiley-VCH: Weinheim, DE, 2004.

(5) Zhou, H.; Yea, Q.; Xu, J. Polyhedral Oligomeric Silsesquioxane-Based Hybrid Materials and their Applications. *Mater. Chem. Front.* **2017**, *1*, 212−230.

(6) Ayandele, E.; Sarkar, B.; Alexandridis, P. Polyhedral Oligomeric Silsesquioxane (POSS)-Containing Polymer Nanocomposites. *Nanomaterials* **2012**, *2*, 445−475

(7) Raftopoulos, K.N.; Pielichowski, K. Segmental Dynamics in Hybrid Polymer/POSS Nanomaterials. *Progress in Polymer Science* **2016**, *52*, 136–187.

(8) Kuo, S.W. Building Blocks Precisely from Polyhedral Oligomeric Silsesquioxane Nanoparticles. *ACS Central Science* **2016**, *2*, 62−64.

(9) Kuo, S.W.; Chang, F. C. POSS Related Polymer Nanocomposites. *Progress in Polymer Science* **2011**, *36*, 1649–1696.

(10) Fina, A.; Monticelli, O.; Camino, G. POSS-Based Hybrids by Melt/Reactive Blending. *J. Mater. Chem.* **2010**, *20*, 9297–9305.

(11) Tanaka, K.; Chujo, Y. Advanced Functional Materials Based on Polyhedral Oligomeric Silsesquioxane (POSS). *J. Mater. Chem.* **2012,** *22*, 1733−1750.

(12) D'Arienzo, M.; Redaelli, M.; Callone, E.; Conzatti, L.; Di Credico, B.; Dirè, S.; Giannini, L.; Polizzi, S.; Schizzi, I.; Scotti, R.; Tadiello, L.; Morazzoni, F. Hybrid SiO_2@POSS Nanofiller: a Promising Reinforcing System for Rubber Nanocomposites. *Mater. Chem. Front.* **2017**, *1*, 212–230.

(13) Redaelli, M.; D'Arienzo, M.; Brus, J.; Di Credico, B.; Geppi, M.; Giannini, L.; Matejka, L.; Martini, F.; Panattoni, F.; Spirkova, M.; Šlouf, M.; Scotti, R.; Morazzoni, F. On the Key Role of SiO_2@POSS Hybrid Filler in Tailoring Networking and Interfaces in Rubber Nanocomposites. *Polymer Testing.* **2018**, *65,* 429–439

(14) Cordes, D. B.; Lickiss P. D.; Rataboul, F. Recent Developments in the Chemistry of Cubic Polyhedral Oligosilsesquioxanes. *Chem. Rev.* **2010***, 110,* 2081–2173.

(15) Dirè, S.; Borovin, E.; Ribot, F. *"Architecture of Silsesquioxanes". In Handbook of Sol-Gel Science and Technology*; Klein, L.; Aparicio, M.; Jitianu, A., Eds.; Springer: New York, NY, 2016, 1–34.

(16) Choi, S.; Lee, A. S.; Hwang, S. S.; Baek, K. Structural Control of Fully Condensed Polysilsesquioxanes: Ladderlike vs Cage Structured Polyphenylsilsesquioxanes. *Macromolecules* **2015**, *48*, 6063−6070.

(17) Matějka, L.; Amici Kroutilová, I.; Lichtenhan, J. D.; Haddad, T. S. Structure Ordering and Reinforcement in POSS Containing Hybrids. *European Polymer Journal* **2014**, *52*, 117–126.

(18) Brown, F.; Vogt, L. H.; Katchman, A.; Eustance, J.; Kiser, K. M.; Krantz, K. W. Double Chain Polymers of Phenylsilsesquioxane. *J. Am. Chem. Soc.* **1960**, *82*, 6194−6195.

(19) Yamamoto, S.; Yasuda, N.; Ueyama, A.; Adachi, H.; Ishikawa, M. Mechanism for the Formation of Poly(phenylsilsesquioxane). *Macromolecules* **2004**, *37*, 2775−2778.

(20) Lee, A. S.; Choi, S. S.; Lee, H. S.; Baek, K. Y.; Hwang, S. S. A New, Higher Yielding Synthetic Route Towards Dodecaphenyl Cage Silsesquioxanes: Synthesis and Mechanistic Insights. *Dalton Trans.* **2012**, *41*, 10585−10588.

(21) Lee, A. S.; Choi, S. S.; Lee, H. S.; Baek, K. Y.; Hwang, S. S. High Photo- and Electroluminescence Efficiencies of Ladder-Like Structured Polysilsesquioxane with Carbazole Groups. *J. Mater. Chem.* **2010**, *20*, 9852−9854.

(22) Choi, S. S.; Lee, A. S.; Lee, H. S.; Jeon, H. Y.; Baek, K. Y.; Choi, D. H.; Hwang, S. S. Synthesis and characterization of UV-Curable Ladder-Like Polysilsesquioxane. *J. Polym. Sci., Part A: Polym. Chem.* **2011***, 49*, 5012−5018.

(23) Lee, A. S.; Lee, J. H.; Lee, J.; Hong, S. M.; Hwang, S. M., Min Koo, C. Novel Polysilsesquioxane Hybrid Polymer Electrolytes for Lithium Ion Batteries. *J. Mater. Chem. A.* **2014**, *2*, 1277−1283.

(24) D'Arienzo, M.; Diré, S.; Redaelli, M.; Borovin, E.; Callone, E.; Di Credico, B.; Morazzoni, F.; Pegoretti, A.; Scotti, R. Unveiling the Hybrid Interface in Polymer Nanocomposites Enclosing Silsesquioxanes with Tunable Molecular Structure: Spectroscopic, Thermal and Mechanical Properties. *Journal of Colloid and Interface Science* **2018**, *512*, 609-617

(25) Cho, K. Y.; Lee, A. S.; Jeon, H.; Park, S.; Jang, M.; Yoon, M.; Hong, S.; Baek, K.; Hwang, S.S.Tuning the Interface Between Poly(vinylidene fluoride)/UV-Curable Polysilsesquioxane

Hybrid Composites: Compatibility, Thermal, Mechanical, Electrical, and Surface Properties. *Polymer* **2015**, *77*, 167−176.

(26) Prateek; Thakur, V. K.; Gupta, R. K. Recent Progress on Ferroelectric Polymer-Based Nanocomposites for High Energy Density Capacitors: Synthesis, Dielectric Properties, and Future Aspects. *Chem. Rev.* **2016**, *116 (7)*, 4260–4317

(27) Liu, L. L.; Yuan, Y.; Huang, Y.; Yub, H.; Yanga, J. A New Mechanism for the Low Dielectric Property of POSS Nanocomposites: the Key Role of Interfacial Effect. *Phys. Chem. Chem. Phys.* **2017**, *19*, 14503–14511

(28) Yang, B.; Xu, H.; Yang, Z.; Liud, X. Design and Architecture of Low-Dielectric-Constant Organic–Inorganic Hybrids from Octahydridosilsesquioxanes. *J. Mater. Chem.* **2009**, *19*, 9038–9044

(29) Massiot, D.; Fayon, F.; Capron, M.; King, Ian. Modelling One and TwoDimensional SolidState NMR Spectra. *MRC.* **2002**, *40*, 70–76.

(30) Martìnez-Richa, A.; Silvestri R. Solid-State NMR Spectroscopy of Multiphase Polymer Systems. Cap. 13 in Handbook of Multiphase Polymer Systems; Boudenne, A.; Ibos, L.; Candau, Y.; Thomas, S., Eds; John Wiley and Sons Ltd: Chichester, U.K., 2011.

(31) Scholz, J.; Etter, M.; Haas, D.; Meyer, A.; Kornowski, A.; Sazama, U.; Mascotto, S. Pore geometry effect on the synthesis of silica supported perovskite oxides. *Journal of Colloid and Interface Science*, **2017**, *504*, 346−355

(32) Unno, M.; Matsumoto, T.; Matsumoto, H., Synthesis of Laddersiloxanes by Novel Stereocontrolled Approach. *J. Organomet. Chem.* **2007**, *692*, 307−312.

(33) Borovin, E.; Callone, E.; Papendorf, B.; Guella, G.; Dirè, S. Influence of Sol-Gel Conditions on the Growth of Thiol-Functionalized Silsesquioxanes Prepared by In Situ Water Production. *J. Nanosci. Nanotech.* **2016**, *16*, 3030–3038.

(34) Zhang, Z. X.; Hao, J; Xie, P.; Zhang, X; Han, C.C.; Zhang, R. A Well-Defined Ladder Polyphenylsilsesquioxane (Ph-LPSQ) Synthesized via a New Three-Step Approach: Monomer Self-Organization−Lyophilization—Surface-Confined Polycondensation. *Chemistry of Materials* **2008**, *20*, 1322–1330

(35) Prado, L. A. S. De A.; Radovanovic, E.; Pastore, H. O.; Yoshida, I. V. P.; Torriani, I. L. Poly(phenylsilsesquioxane)s: Structural and morphological characterization. *Journal of Polymer Science: Part A: Polymer Chemistry* **2000**, *38*, 1580–1589

(36) Di Maggio, R.; Callone, E.; Girardi, F.; Diré, S. StructureRelated Behavior of Hybrid Organic–Inorganic Materials Prepared in Different Synthesis Conditions from ZrBased NBBs and 3-Methacryloxypropyl trimethoxysilane. *Journal of Applied Polymer Science* **2012**, *125*, 1713–1723.

(37) Gibin, G.; Prof. Lorenzetti, A.; Dr. Callone, E.; Dirè, S.; Dolcet, P.; Venzo, A.; Causin, V.; Marigo, A.; Modesti, M.; Gross, S. Smart and Covalently CrossLinked: Hybrid Shape Memory Materials Reinforced through Covalent Bonds by Zirconium Oxoclusters. *ChemPlusChem* **2016**, *81*, 338 –350

(38) Ferrini, V.; Forte, C.; Geppi, M.; Pizzanelli, S.; Veracini, C. A. Correlation Between ^{1}H FID and $T_{1\rho}$ Components in Heterogeneous Polymer Systems: an Application to SBS. *Solid State Nucl. Magn. Reson.* **2005**, *27*, 215–222.

(39) Beaucage, G. Approximations Leading to a Unified Exponential/Power-Law Approach to Small-Angle Scattering. J. Appl. Cryst. **1995**, *28*, 717–728

(40) Beaucage, G. Small-Angle Scattering from Polymeric Mass Fractals of Arbitrary Mass-Fractal Dimension. J. Appl. Cryst. **1996**, *29*, 134–146

(41) Pecharroman, C.; Moya, J. S. Experimental Evidence of a Giant Capacitance in Insulator–Conductor Composites at the Percolation Threshold. *Adv. Mater.* **2000***, 12*, 294–297.

(42) Dang, Z.-M.; Fan, L.-Z.; Shen, Y.; Nan, C.-W. Study on Dielectric Behavior of a Three-Phase CF/(PVDF + $BaTiO_3$) Composite. *Chem. Phys. Lett.* **2003***,369*, 95–100.

(43) Bergman, D. J.; Imry, Y. Critical Behavior of the Complex Dielectric Constant near the Percolation Threshold of a Heterogeneous Material. *Phys. Rev. Lett.* **1977**, *39*, 1222.

(44) Qi, L.; Lee, B. I.; Chen, S.; Samuels, W. D.; Exarhos, G. J. High-Dielectric-Constant Silver–Epoxy Composites as Embedded Dielectrics. *Adv. Mater.* **2005**, *17*, 1777–1781.

(45) Crippa, M.; Bianchi, A.; Cristofori, D.; D'Arienzo, M.; Merletti, F.; Morazzoni, F.; Scotti, R.; Simonutti, R. High Dielectric Constant Rutile-Polystyrene Composite with Enhanced Percolative Threshold. *J. Mater. Chem. C* **2013**, 1, 484–492.

(46) Dang, Z. M.; Wu, J. P.; Xu, H. P.; Yao, S. H.; Jiang, M. J. Dielectric Properties of Upright Carbon Fiber Filled Poly(vinylidene fluoride) Composite with Low Percolation Threshold and Weak Temperature Dependence. *Appl. Phys. Lett.* **2007**, *91*, 072912.

(47) Grannan, D. M.; Garland, J. C.; Tanner, D. T. Critical Behavior of the Dielectric Constant of a Random Composite near the Percolation Threshold. *Phys. Rev. Lett.* **1981**, *46*, 375.

(48) Dang, Z. M.; Lin, Y. H.; Nan, C. W. Novel Ferroelectric Polymer Composites with High Dielectric Constants. *Adv. Mater.* **2003**, *15*,1625–1629.

(49) Jylha, L.; Sihvola, A. Equation for the Effective Permittivity of Particle-Filled Composites for Material Design Applications. *J. Phys. D: Appl. Phys.* **2007**, *40*, 4966–4973.

SYNOPSIS

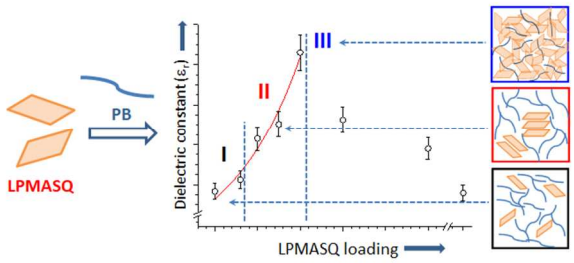
LPMASQ
PB
Dielectric constant (ε_r)
I
II
III
LPMASQ loading